RSC Advances

PAPER

View Article Online
View Journal | View Issue

Cite this: *RSC Adv.*, 2023, **13**, 25369

Synthesis of an aggregation-induced emission-based fluorescent probe based on rupestonic acid†

Zhichao Cui,[a] Yucai Zhang,[a] Zhonghui Zhang,[b] Adila Abudurexiti*[a] and Abdulla Yusuf *[a]

Received 26th May 2023
Accepted 14th August 2023

DOI: 10.1039/d3ra03521b

rsc.li/rsc-advances

Chinese herbal medicine and Chinese patent medicine have been widely applied for cancer care in China. Rupestonic acid, an active ingredient of *Artemisia rupestris* L., has recently been confirmed to have certain anti-tumor effects *in vitro*. In this study, we employed the application of a commonly devoted triphenylamine as a fluorophore and the addition of 2,4-thiazolidinedione as a bridge to integrate rupestonic acid into the AIE system to create an fluorescent probe with anti-tumor properties. The spectral, cytotoxic, and cellular imaging properties of the probe were measured. Its promising responses make possible the application of the probe in antitumor theragnostic systems.

1. Introduction

Fluorescence has been used in biological research for the last 100 years, although developments in fluorescence chemistry, along with technical discoveries, have fueled the development of many different kinds of fluorophores. The use of fluorescent molecules in biological research is the standard in many applications and their use is continually increasing due to their versatility, sensitivity and quantitative capabilities. The vast selection of fluorophores today provides greater flexibility, variation and fluorophore performance for research applications than ever before. Researchers have prioritized the development of research applications for luminescent materials due to their visualization properties.[1–3] Fluorescent probes among organic luminescent materials are playing an increasingly important role in biomedicine, biological chemistry, and life sciences.[4–8] Aggregation-induced emission (AIE) is a new concept created in 2001 by B. Z. Tang to describe a photophysical phenomenon, in which non-emissive molecules in solutions are induced to emit strongly when their intramolecular motion is restricted in the aggregate or solid state.[9,10] The concept of AIE describes a phenomenon whereby emission is observed when the luminogen aggregates with other molecules. Typically, this luminogen is originally non-emissive or weakly emissive due to molecular motions, which allow the molecule to decay nonradiatively. Upon aggregation or binding to molecules, such molecular motions become restricted, forcing the molecule to decay *via* radiative pathways, turning on emission.[11] Aggregation-induced emission (AIE) probes are a series of significant luminescent materials.[12,13] AIE probes plays an important role in the early detection and treatment of cancer due to low toxicity and low susceptibility to drug resistance.[14–18] AIE combines the advantages of high biocompatibility, degradability and bioactivity of natural products, and has important value in designing novel structures, innovating the research into drug activity mechanisms of natural products, and promoting the application of AIE materials.

Data from the International Agency for Research on Cancer show that cancer is one of the leading causes of human death.[19–21] By 2040, worldwide cancer cases will increase by 60%, while this will be ~81% in developing countries, according to the latest report of the World Health Organization (WHO).[22] Breast cancer ranks first in the incidence of malignant tumors among women in China, making it one of the most common malignant tumors encountered in clinical practice.[23,24] Triple-negative breast cancer (TNBC), which accounts for 20% of all new cases of breast cancer, is a subtype of the disease that lacks the genes for the estrogen receptor (ER), progesterone receptor (PR), and human epidermal growth factor receptor-2 (Her2/neu). According to clinical, genomic, and transcriptomic data in China, TNBCs was classified into four transcriptome-based subtypes: (1) luminal androgen receptor (LAR), (2) immunomodulatory, (3) basal-like immune-suppressed, and (4) mesenchymal-like.[25] The differential diagnosis of TNBC metastases and primary cancers from other organs can be difficult due to lack of a TNBC standard immune profile. There are some imaging techniques, such as ultrasound, X-ray, computed tomography (CT), magnetic resonance imaging (MRI), and positron emission tomography (PET), using for diagnosis and adjuvant therapy in TNBC and other cancer treatment. The traditional imaging technique like X-ray, CT, MRI or PET give

[a]*College of Chemistry and Environmental Science, Laboratory of Xinjiang Native Medicinal and Edible Plant Resources Chemistry, Kashi University, Kashi 844000, China. E-mail: kashidaxue_abudula@163.com; Tel: +86-18690293325*

[b]*Guangdong Key Laboratory of Chiral Molecule and Drug Discovery, School of Pharmaceutical Sciences, Sun Yat-sen University, Guangzhou 510006, China*

† Electronic supplementary information (ESI) available. See DOI: https://doi.org/10.1039/d3ra03521b

a powerful assistance to physicians to screen tumor tissue of patients or to localize lesions more precisely. These imaging techniques make it possible for surgical planning or interim assessment. In addition, these techniques also guide surgery and the delivery of radiotherapy to improve precision and allow non-invasive monitoring of patients' response to therapy.[26] Traditional mammography, ultrasound and magnetic resonance imaging are difficult to diagnose due to lack of characteristics.[27] Despite the significant resources spent on TNBC research in humans, gaps in the early preventive detection of the disease currently exist.[28–31] Early diagnosis and effective treatment of TNBC can lower the cost of cancer care while easing the burden and suffering of patients. Fortunately, fluorescence imaging (FLI) has shown great potential for guiding surgeons during complex interventions.[32]

In addition to traditional cancer treatment schemes, natural products are still an important source of treatment due to their structural diversity and unique biological activities.[33,34] The discovery of new anti-cancer roles of natural products marks an upsurge in exploring and harnessing nature in human medicine.[35] Chinese herbal medicine and Chinese patent medicine have been used in clinical treatment, *e.g.*, *Rabdosia rubescens* (Hemsl.) Hara, *Salvia miltiorrhiza*, and extracts, which have been increasingly used in treatment of tumors.[36,37] Tumor targeting and imaging are important endeavors in the area of biomedical research. In terms of FLI technology, new AIE fluorescent probes play a key role and whose development may revolutionize the cell imaging and diagnose field. Specially designed AIE fluorescence probes have been utilized for various biomedical imaging applications, thanks to their high emission efficiency and superb photobleaching resistance.[38] However, it is difficult for traditional natural drugs to undertake the important task of detection due to their weak fluorescence, many chiral groups and weak conjugation effect. The natural product AIE probe that undertakes the detection of tumor cells is rarely known. Therefore, it is extremely important to develop a new type of natural product AIE probe with novel structure and both diagnosis and treatment of cancer.

Triphenylamine (TPA) itself does not emit light, but can form a helical structure, which is very conducive to the construction of AIE compounds. Triphenylamine itself also has a strong electron donating ability.[39–41] By combining triphenylamine with electron withdrawing groups can regulate intramolecular function of pushing and pulling electrons achieves the purpose of regulating light emission. Thiazolidinedione derivatives have attracted a significant amount of attention from the medical community for their excellent physiological effects and mechanisms of action.[42–44] Rupestonic acid is a monoterpene monomeric compound isolated from *Artemisia rupestris* L., a characteristic medicinal plant from Xinjiang used for anti-allergic, anti-tumor, anti-inflammatory, and detoxification purposes.[45] In our previous research, we used MDA-MB-231 cell line representing triple-negative breast cancer to measure anti-tumor activity of isolated rupestonic acid. Our cell panel research shows that rupestonic acid has potential anti-tumor activity to MDA-MB-231 cell with inhibition rate 86.5% (in 20 μM).

The current research on natural products and TNBC has mainly focused on suppressing the expression of specific genes in this cell line or increased the expression of genes that control apoptosis, which has led to the progression of cancer cells toward apoptosis. In this study, we employed the application of a commonly devoted triphenylamine as a fluorophore and the addition of 2,4-thiazolidinedione as a bridge to integrate rupestonic acid into the AIE system. The probe was subjected to optical testing, *in vitro* anti-tumor testing, molecular docking and cellular imaging.

2. Results and discussion

2.1. Design and synthesis of the probe (M5-0)

The isolated rupestonic acid shows anti-tumor activity to MDA-MB-231 cell with inhibition rate 86.5% (in 20 μM). However, the compound has no fluorescence properties which makes it difficult to study its drug action mechanism. Triphenylamine always used as fluorophore in AIE system. We designed an AIE probe based on rupestonic acid used 2,4-thiazolidinedione as linker and triphenylamine as a fluorophore.

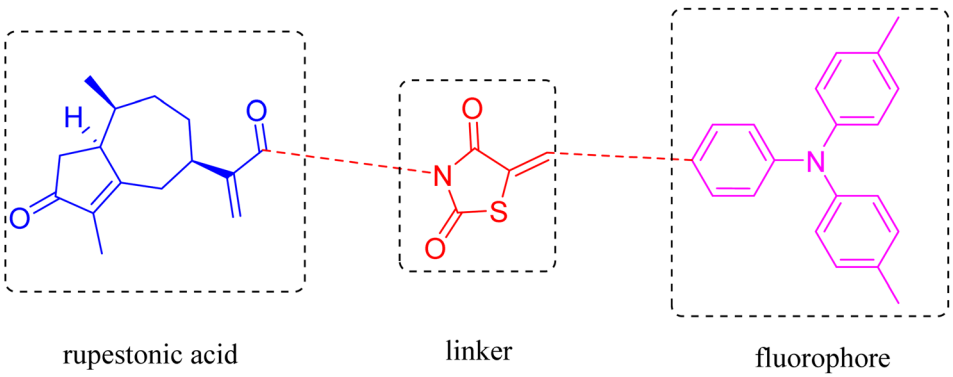

2.2. Spectroscopic testing of the probe (M5-0)

2.2.1. Ultraviolet absorption spectroscopy. We measured the ultraviolet absorption spectroscopy of the probe in three hydrophilic solvents, THF, MeOH and DMSO. The maximum absorption peak was at 425 nm (Fig. 1). Although the absorption intensity of the probe in THF was stronger than in MeOH and DMSO, we chose methanol as the solvent for subsequent research due to the better solubility of the probe in methanol.

2.2.2. Fluorescence testing of M5-0. Triphenylamine is a typical AIE-type compound, and the aimed probe molecule in this paper contains a derivative of triphenylamine, so it is necessary to investigate the AIE properties of this molecule. Fluorophore emission can be directly influenced by interaction with other fluorescent or non-fluorescent molecules, which can "quench" the emitted fluorescence from the excited fluorophore. When most common chromophores are in the aggregation state with high con-centration, aggregation-caused quenching (ACQ) will occur, which seriously limits the application of probes in sensors and biology. Natural products often have picky solubility. The probe we developed based on isolated rupestonic acid need to screen the suitable solvent in this research at first.

Emission wavelengths are specific characteristics of fluorescent probe. It is important to choose a suitable solvent for the probe, at first. To investigate the most suitable solvent for AIE emission, we tested the fluorescence emission of **M5-0** under different solvent, ethyl acetate, dichloromethane, tetrahydrofuran, DMSO, acetonitrile, MeOH, and H_2O. The fluorescence data shows that THF and H_2O was not the proper solvent for **M5-0**. The fluorescence emission intensity under pure solvent conditions in that order: H_2O > THF > EA > DCM > DMSO > ACN > MeOH (Fig. 2A and B). Given the above reasons, methanol was chosen as the most suitable solvent for **M5-0**.

We observed the fluorescence of the **M5-0** with the naked eye in MeOH/water mixture solvent with different fraction of water (f_w) at 365 nm (Picture 1). It can easily find that when f_w is 0–40%, there is no fluorescence phenomenon. When the f_w further increases to 60%, a clear fluorescence phenomenon can be observed and the probe demonstrated colorimetric orange fluorescence. As the f_w increases to 80%, the fluorescence clearly turns bright yellow, and the f_w further increases to 90%, making the fluorescence appear stronger. In the high-volume fraction aqueous phase, the probe exhibits stronger fluorescence. We have designed more experiments to confirm the experimental phenomena observed with the naked eye.

As shown in the Fig. 3, **M5-0** have gradient changes in fluorescence in MeOH/water mixture solvent with different fraction of water. In a higher volume fraction water, the fluorescence intensity is positively correlated with the f_w. When the f_w <40%, there is almost no fluorescence emission. When the f_w going to 60%, the fluorescence emission intensity significantly increases. As the volume of water further increases, the fluorescence emission coming stronger. **M5-0** is AIE emission in higher polar solvents, that phenomenon is the typical characteristic of AIE fluorescent probes. The brightness of a given fluorophore is determined by the quantum yield. The quantum

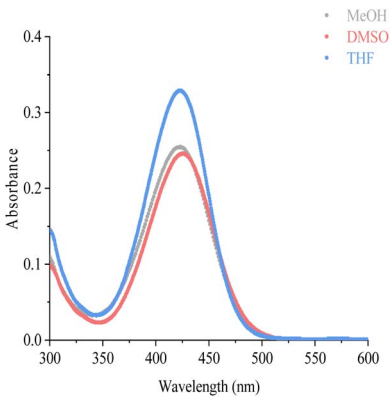

Fig. 1 The UV spectroscopy of **M5-0** in THF, MeOH, DMSO (c = 10 μM, λ_{max} = 425 nm).

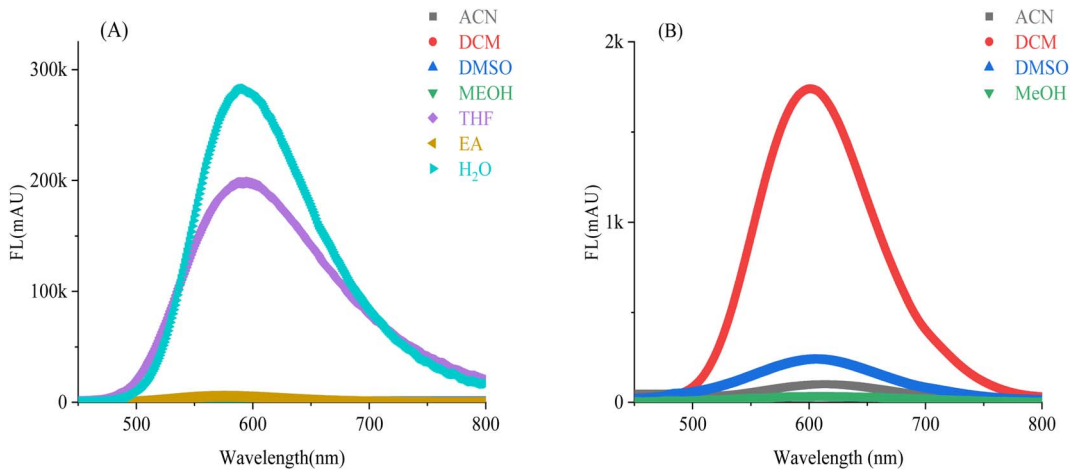

Fig. 2 Fluorescence data of probe **M5-0**, (A) fluorescence emission of the probe under different solvents, (10 μM, λ_{mex} = 420 nm); (B) partial enlarged view of (A) (vertical coordinate 200× enlarged).

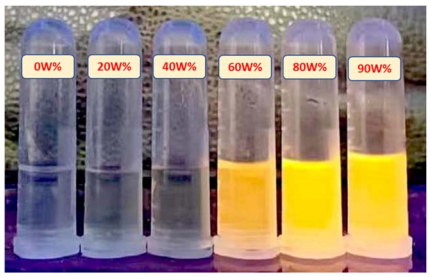

Scheme 1 The AIE fluorescence of **M5-0** in MeOH/water mixture solvent, from left to right the f_w was 0%, 20%, 40%, 60%, 80%, 90%, respectively (c = 10 μM, λ = 365 nm).

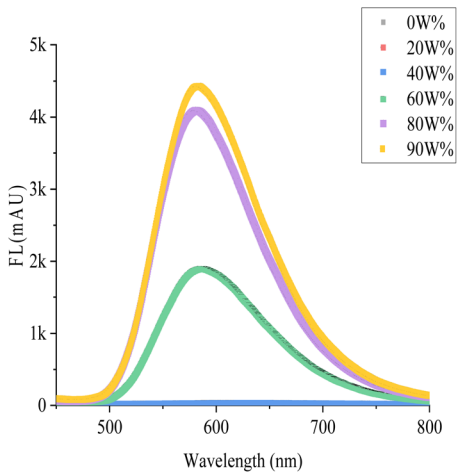

Fig. 3 PL spectra of probe **M5-0** in MeOH/water mixture solvent (10 μM, λ_{mex} = 420 nm).

yield is calculated as the number of photons that are emitted by the fluor divided by the number of photons that are absorbed. In pure MeOH, the quantum yield (QYs) of the probe is 0.92%, while in water, the QYs of the probe is 20.34%, which is an increase of 22 times.

2.3. Inhibition of the probe M5-0 on MDA-MB-231 cells

Cell viabilities of Triple-negative breast cancer cells (MDA-MB-231) and normal cells were measured, and the results are shown in Fig. 4. The survival rate of these cells was calculated to be 100.00% in normal iterative culture without the addition of probe molecules, *i.e.*, no inhibition at all (variance of 0.0532). The probe had almost no inhibitory effect on the entire cell population after 48 hours of incubation at a probe concentration no greater than 20 μM, with the survival rate 99.20% (1 μM, variance: 0.0363), 97.97% (10 μM, variance: 0.0135), and 96.32% (20 μM, variance: 0.0572). The latent therapeutic effectiveness of the probe on the cells was confirmed when the concentration of the probe was raised above 40 μM, since this caused a sharp decline in cell survival and an increase in the degree of cancer cell inhibition. At 40 μM, the cell survival rate was 62.42% (variance: 0.0829), while the probe concentration reached to 80 μM, the survival rate decreased to 28.22% (variance: 0.1195). At

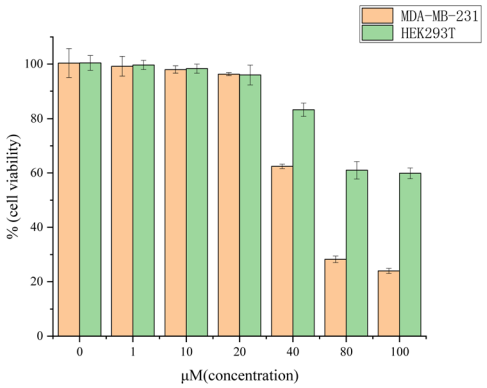

Fig. 4 Cell viabilities of MDA-MB-231 cells and HEK293T cells after incubation with different concentrations of **M5-0**.

100 μM, the cell survival rate was the lowest with 23.92% (variance: 0.0940). In summary, the probe has low cytotoxicity at low concentrations (concentrations less than 20 μM) and can be used for live cell imaging; Above this concentration, it can also inhibit cancer cells, which is the unique feature of this probe. Encouragingly, although it exhibits toxicity to normal cells at high concentrations (concentration higher than 40 μM), it is lower in toxicity to cancer cells.

2.4. Molecular docking

In silico has advantages over *in vitro* experiments which are often time-consuming, require significant resources, and are vulnerable to failure. The save of time and resources is remarkable when *in silico* predictions are carried out before the compound is tested *in vitro* and *in vivo*.[46] Molecular docking studies were carried out to provide a theoretical viewpoint on potential molecular interactions between both rupestonic acid and the probe with target proteins. The Janus kinase 2 protein was chosen to investigate rupestonic acid and the probe's anticancer activities on breast cancer considering the protein was targeted by many anti-cancer drugs to produce their response.[47,48]

Rupestonic acid and the probe exhibited hydrogen bond with ASP939 and ARG980 residues, respectively (Fig. 5a and b). It can be seen that the probe and amino acid residues ARG980 can form three hydrogen bonds [the oxygen atoms on the carbonyl group of rupestonic acid and carbonyl group of thiazolidinedione form three hydrogen bonds respectively, (b)] when rupestonic acid and residues ASP939 form one hydrogen bond [the oxygen atom on the carbonyl group of rupestonic acid and the hydrogen on the amino acid residue form a hydrogen bond, (a)]. However, the Glide score of the probe (−4.187) is higher than rupestonic acid (−6.069), this may be caused by the high resistance of probe. We can find a convincing answer from the two figures c and d. It is obviously seen that the probe partially entered in the protein site (d) while rupestonic acid filled the site smoothly (c).

2.5. Cell imaging

Live-cell imaging applies to a wide range of biological applications, including basic and medical research. Spectroscopic

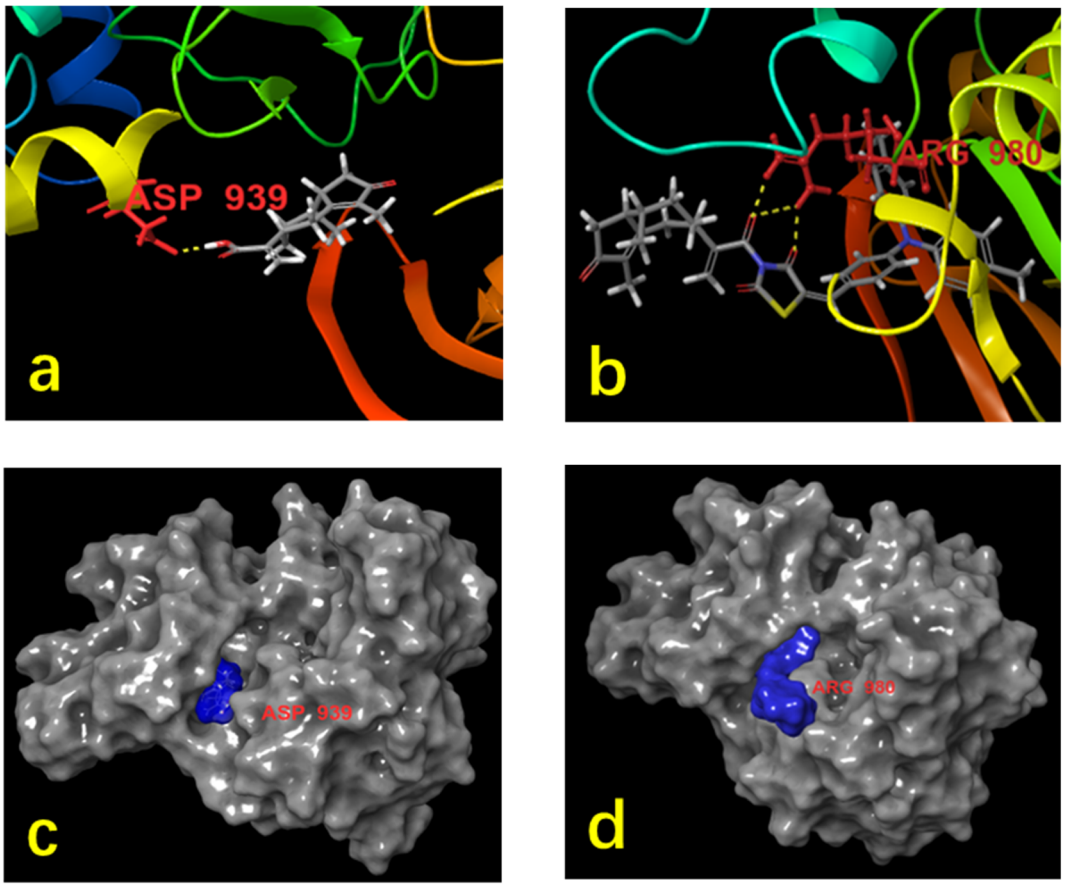

Fig. 5 Molecular interactions of rupestonic acid and the ASP939 residues (a); molecular interactions of probe and the ARG980 residues (b); binding site surface of rupestonic acid and the target protein (c); binding site surface of probe and the target protein (d).

experiments have demonstrated the probe molecule **M5-0** characteristics, although cellular testing is still essential. We investigated the probe's effectiveness in cells and revealed that the fluorescent compound **M5-0** inhibits the growth of MDA-MB-231. We also attempted to explore the application of the probe in MDA-MB-231 cell imaging. First, MDA-MB-231 cells were photographed using an **M5-0** solution containing various concentrations of the probe molecule (Fig. 6, this figure is partially zoomed in views of the fluorescence image, for original picture please see ESI† Fig. 10–13).

Without the insertion of the probe, there was no background interference in the MDA-MB-231 cells, and the cells showed typical spindle cone structure. The fluorescence image showed a complete cell outline and a modest alteration in the cell shape at a probe concentration of 10 μM, the cells are evenly stained, the outline of the nucleus can be clearly seen, and the cells are in normal physiological state. When the probe concentration reached 20 μM, the cell is still remaining a normal tubular cell shape, the probe shows stronger fluorescent highlights, the nucleus outline is also clearly seen. When the probe concentration increased to 40 μM, the cell morphology starts from a normal spinning cone to an abnormal spherical state, the outline of the cell membrane begins to blur, the volume of the nucleus becomes larger and fluorescence of the probe in cell is decreasing obviously. At higher concentrations as 80 μM and 100 μM, most of the cells have been lose viability and float in the culture medium, making the cell outline difficult to see clearly. Secondly, in terms of cell state, it is difficult to quantify the inhibitory effect of high concentration probe on cells, so we use CCK-8 method to conduct cell viability experiment with the probe as the drug itself.

As a naturally occurring active monomer isolated from the plant Artemisia, research on it has been stalled in the areas of pharmacological structural modification in chemistry and *in vitro* activity testing in biology. Applied research on its detection and cell imaging is also at a standstill, and after consulting a large number of references, only active-site modification can be resolved. Additionally, it is nearly impossible to locate the procedure for determining the entire effective monomer and the fluorescent molecule when browsing through other sources. First, the current standard of care involves using the drug-carrying portion of a well-studied drug-molecule monomer. Accessing a fluorescent molecule that does not contain many double bonds or a benzene-ring conjugation system is a very dangerous but worthwhile process. Second, due to its long cycle time and high failure rate, pharmaceutical research, particularly natural product research, has not received the attention it merits. With this in mind, we seek to create a more open

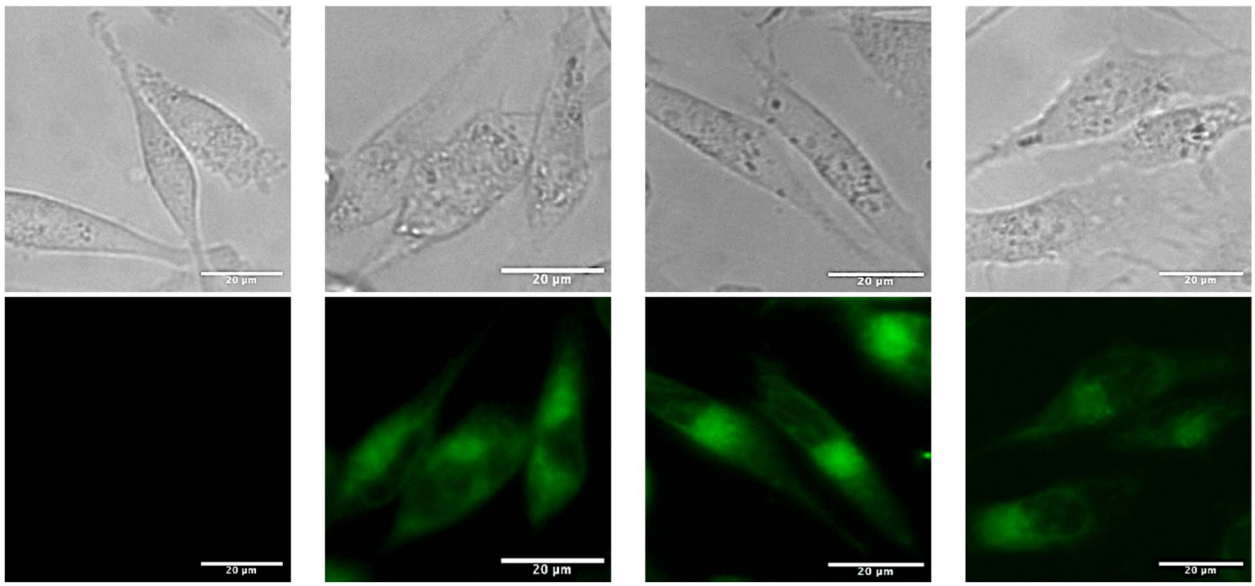

Fig. 6 Fluorescence imaging of live cells (MDA-MB-231) with probe molecule **M5-0** (from left to right probe concentrations are 0 μM, 10 μM, 20 μM, 40 μM in that order).

interdisciplinary bridge between pharmacological and biological research.

Most likely as a result of rupestonic acid's non-conjugated nature, two large fatty rings comprise the structure of that compound, and only the carbonyl group above the carboxyl group and the nearby double bonds are involved in the AIE group conjugation, while the other fatty rings weaken the initial conjugation system. However, this structure also serves as a reminder that, when designing a natural product probe molecule, one should consider the conjugation of the loaded drug molecule and give priority to the probe's structure simplification and ability to be taken orally. To lessen the weakened fluorescence effect of the drug-molecule cluster, the design of the probe molecule should take into account the conjugation of the loaded drug molecule. Additionally, when choosing a structure, it is preferable to simplify the structure and allow access to the effective portion of the original drug molecule. This study provides valuable reference for the future development of fluorescent probes based on natural product.

3. Materials and methods

3.1. Materials

All chemicals were purchased from commercial suppliers and used without further purification. The purity of rupestonic acid and **M5-0** were determined by high performance liquid chromatography (Waters Acquity Arc), and purity of other synthesized compounds were confirmed by thin-layer chromatography (TLC) using several solvent systems of different polarities. ^{1}H NMR, ^{13}C NMR were measured on a Bruker AVANCE II 500 MHZ. Digital NMR Spectrometer with tetramethyl silane (MS) as internal standard and DMSO-d_6 as diluent. Mass spectra were measured on a Waters UPLC-MS. UV-vis spectra were recorded on a UV-2600i (A12595931269) at 25 °C. Melting points of compounds were measured by METTLER TOLEDO MP70 Melting Point System. Fluorescence measurements were carried out using an Edinburgh Instruments FLS1000 fluorescence spectrophotometer. Confocal fluorescence images were recorded using a Thermo Fisher Invitrogen™ EVOS™ FL Auto 2.

3.2. Isolation of rupestonic acid

About 1 kg of *A. rupestris* L. (commercially available, purchased from Baokang Pharmaceutical Co., Ltd) were extracted three times with 75% ethanol (reflux 1, 2 and 3 h respectively). The extracts were combined and evaporated to dryness under reduced pressure, which yield 0.18 kg of extract. The extract was dissolved in 1 L water, and extract three times with EA. Combine the organic phase and adjust pH to 8 by adding 5% $NaHCO_3$. After separating the aqueous phase, add dilute hydrochloric acid and adjust the pH value to 3. Aqueous phase extract three times with EA and the combined organic phase evaporated under reduced pressure. Obtain crude products purified by column chromatography (petroleum ether : ethyl acetate = 5 : 1), and recrystallization with acetone to give 0.8 g pure rupestonic acid (purity >98%, mp: 132.7–134.2 °C). ^{1}H NMR (500 MHz, $CDCl_3$) δ 6.35 (s, 1H), 5.71 (s, 1H), 3.24–3.08 (m, 1H), 2.90–2.88 (m, 1H), 2.86–2.84 (m, 1H), 2.64–2.63 (m, 1H), 2.49–2.41 (m, 1H), 2.15 (s, 2H), 2.13–2.08 (m, 1H), 2.05–2.03 (m, 1H), 1.81 (s, 3H), 1.62–1.58 (m, 3H), 0.63 (d, J = 7.1 Hz, 3H). ^{13}C NMR (125 MHz, $CDCl_3$) δ 208.85, 175.20, 171.32, 145.75, 137.77, 125.33, 46.00, 41.30, 38.39, 37.69, 36.55, 35.27, 31.57, 12.11, 8.00.

3.3. The synthesis of M5-0

3.3.1 Synthesis of (*E*)-5-(4-(di-*p*-tolyl amino) benzylidene) thiazolidine-2,4-dione (M5-2). To a stirred solution of **M5-1** (500 mg, 1.66 mmol), 2,4-Thiazolidinedione (214 mg, 1.83 mmol), acetic acid (5 mg, 0.083 mmol), 3-picoline (7.7 mg, 0.083

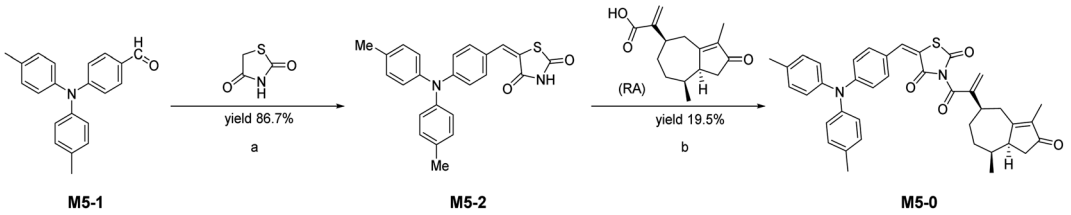

Fig. 7 Synthetic route for probe **M5-0**: (a) 2,4-thiazolidinedione, acetic acid, 3-picoline, toluene (b) rupestonic acid, DIEA, HATU, DCM.

mmol) in toluene (15 mL) was refluxed for 16 h. The reaction was concentrated under a vacuum pump and purified by chromatography on silica gel (EtOAc : PE = 1 : 10) to afford **M5-2** (576 mg, red solid, mp: 185.4–186.7 °C). ^{1}H NMR (500 MHz, $CDCl_3$) δ 7.78 (s, 1H), 7.30 (d, J = 9.0 Hz, 2H), 7.13 (d, J = 8.0 Hz, 4H), 7.05 (d, J = 8.4 Hz, 4H), 6.97 (d, J = 9.0 Hz, 2H), 2.34 (s, 6H). ^{13}C NMR (125 MHz, $CDCl_3$) δ 172.34, 171.77, 167.99, 167.58, 150.51, 143.42, 134.59, 131.84, 130.15, 125.95, 123.99, 119.21, 117.21, 20.81 (Fig. 7).

3.3.2 Synthesis of rupestonic acid fluorescent probe (M5-0). A mixture of **M5-2** (268 mg, 0.67 mmol), rupestonic acid (150 mg, 0.61 mmol), and DIEA (236 mg, 1.83 mmol) in dry DCM (10 mL) was stirred. Then HATU (346 mg, 0.91 mmol) was added, and the reaction was carried out for another 72 h. The reaction mixture was concentrated under a vacuum pump and purified by Prep-TLC (EtOAc : PE = 1 : 10) to afford the probe **M5-0** (75 mg, purity 99.42%, orange solid, mp: 192.5–194.1 °C). $C_{39}H_{38}N_2O_4S$: calculated: 630.2552, observed: [M + NH_4^+] = 649.2810. ^{1}H NMR (500 MHz, $CDCl_3$) δ 8.09 (s, 1H), 7.58 (d, J = 5.5 Hz, 1H), 7.44 (d, J = 7.9 Hz, 4H), 7.35 (d, J = 8.0 Hz, 4H), 7.25 (d, J = 8.4 Hz, 2H), 4.65–4.04 (m, 2H), 3.39–3.32 (m, 1H), 3.27–3.14 (m, 2H), 3.03–2.91 (m, 1H), 2.92–2.83 (m, 1H), 2.82–2.72 (m, 1H), 2.65 (s, 6H), 2.43–2.34 (m, 2H), 2.22–2.08 (m, 1H), 1.24–1.12 (m, 1H), 0.91 (d, J = 7.0 Hz, 3H). ^{13}C NMR (125 MHz, $CDCl_3$) δ 209.01, 175.20, 174.99, 168.75, 168.71, 167.03, 167.00, 151.01, 143.85, 138.39, 138.26, 135.14, 135.01, 132.30, 130.66, 126.45, 124.48, 119.63, 116.02, 116.01, 51.03, 46.13, 41.67,41.28 37.40, 36.77, 35.59, 30.05, 21.30, 12.47, 8.44 (Fig. 7).

3.4 Cytotoxicity study

The MDA-MB-231 cells and HEK293T cells in the Petri dish were digested and collected, and the number of cells was calculated and quantified. Each well contained about 5 × 10^3 cells and was inoculated into the 96-well plate. Wells with 1% DMSO volume fraction in cell culture medium (PBS 7.4 (1×), liquid) were used as negative control. Compound **M5-0** was introduced and incubated for 48 hours at a final concentration gradient of 100, 80, 40, 20, 10, and 1 μM. Culture medium was removed and each well received 100 μL of CCK-8 solution that had been diluted 10 times with serum-free medium. After incubation at 37 °C for one hour, OD_{450} in each well was determined under an enzyme-labeled instrument.

3.5. Molecular docking

First, the energy minimization of both rupestonic acid and the probe were performed by ChemBio 3D (calculations → MM2 → minimize energy, keep all of the default settings selected and click "Run" to perform the minimization. Save the resulting compound as a SDF file).[49] Meanwhile, the published X-ray crystallographic structure of MDA-MB-231 polymerase (PDB ID: 3KRR) was downloaded from the PDB database (**https://www.rcsb.org/structure/3KRR**).[47,48] Protein was prepared using the Protein Preparation Wizard tool in maestro molecular modeling software (Schrodinger Release 2018).[50] Finally, molecular docking was carried out by running Ligand Docking tool.

3.6 Bioimaging

The MDA-MB-231 cells in the Petri dish were digested and collected, and the number of cells was calculated and quantified. Each well contained about 4 × 10^4 cells and was inoculated into the 96-well plate. The probe molecules **M5-0** were introduced allowed to work for 2 hours at final concentrations of 10, 20, and 40 μM. Wells with 1% DMSO volume fraction were used as negative control. Culture medium was removed after incubation for 2 hours and each sample was washed three times with 1 mL PBS. The results of intracellular fluorescence imaging were observed and photographed under fluorescence microscope.

4. Conclusions

In this paper, we have successfully developed an aggregation-induced emission-based fluorescent probe based on rupestonic acid. The concept of pharmacological molecule design was incorporated into the luminescence system to build rupestonic acid as probe pharmacophore and triphenylamine as luminescent center. The natural compound-based probe with excellent spectral performance (c = 10 μM) and low cytotoxicity (cell viability with 97.97%, 10 μM, variance: 0.0135) was synthesized and successfully used on cell imaging. Currently, though it is hard to demonstrate with specific data which section or organelle of the cancer cells the probe molecule penetrated, but we have confidence that the above research will provide a solution to the problem of cell co-localization and introduced into antitumor theragnostic systems.

Data availability

Data available in ESI.†

Author contributions

Cui Z. C. accomplished synthesize and writing original paper; Zhang Z. H. carried on the measurement of activity and cell

imaging; Yusuf A completed review, editing and supervision; project administration, Zhang Y. C. and Abudurexiti A. All authors have read and agreed to the published version of the manuscript.

Conflicts of interest

The authors declare no conflict of interest.

Acknowledgements

This research was financially funded by The Key Laboratory Open Project of Xinjiang Uygur Autonomous Region-(2021D04018), Science and Technology Talents Training Project of Tianshan Youth Program of Xinjiang Uygur Autonomous Region (2019Q079) and The Open Project of The Laboratory Xinjiang Native Medicinal and Edible Plant Resources Chemistry (KSUZDSYS202103). We thank Professor Hu W. H. and Professor Xu X. F. (School of Pharmaceutical Sciences, Sun Yat-sen University) for providing experimental research site and research guidance.

References

1 X. Tang, Z. Zhu, R. Liu, L. Ni, Y. Qiu, J. Han and Y. Wang, A novel OFF-ON-OFF fluorescence probe based on coumarin for Al(3+) and F(−) detection and bioimaging in living cells, *Spectrochim. Acta, Part A*, 2019, **211**, 299–305, DOI: 10.1016/j.saa.2018.12.022. https://www.ncbi.nlm.nih.gov/pubmed/30562703.

2 D. Wu, S. Liu, J. Zhou, R. Chen, Y. Wang, Z. Feng, H. Lin, J. Qian, B. Z. Tang and X. Cai, Organic Dots with Large pi-Conjugated Planar for Cholangiography beyond 1500 nm in Rabbits: A Non-Radioactive Strategy, *ACS Nano*, 2021, **15**, 5011–5022, DOI: 10.1021/acsnano.0c09981. https://www.ncbi.nlm.nih.gov/pubmed/33706510.

3 Z. Zong, J. Wang, Y. Bin, Y. Wu and G. Huang, A bifunctional fluorescent probe for sensing of Al^{3+} and H2S, *Anal. Methods*, 2021, **13**, 2157–2164, DOI: 10.1039/d1ay00096a. https://www.ncbi.nlm.nih.gov/pubmed/33884395.

4 L. Cao, J. Xiongn, Y. Wu, S. Ding, M. Li, F. Xie, Z. Ma and Z. Wang, Progress in the Molecular Design and Synthesis of Organic Fluorescent Probe for Picric Acid Detection, *Chin. J. Org. Chem.*, 2016, **36**, 2053–2074, DOI: 10.6023/cjoc201604002.

5 A. C. Sedgwick, L. Wu, H. H. Han, S. D. Bull, X. P. He, T. D. James, J. L. Sessler, B. Z. Tang, H. Tian and J. Yoon, Excited-state intramolecular proton-transfer (ESIPT) based fluorescence sensors and imaging agents, *Chem. Soc. Rev.*, 2018, **47**, 8842–8880, DOI: 10.1039/c8cs00185e, https://www.ncbi.nlm.nih.gov/pubmed/30361725.

6 X. Wang, Y. Zhou, C. Xu, H. Song, X. Pang and X. Liu, A dual-responsive fluorescent probe for detection of fluoride ion and hydrazine based on test strips, *Spectrochim. Acta, Part A*, 2019, **211**, 125–131, DOI: 10.1016/j.saa.2018.12.004, https://www.ncbi.nlm.nih.gov/pubmed/30530065.

7 Y. Wang, Y. F. Song, L. Zhang, G. G. Dai, R. F. Kang, W. N. Wu, Z. H. Xu, Y. C. Fan and L. Y. Bian, A pyrazole-containing hydrazone for fluorescent imaging of Al3+ in lysosomes and its resultant Al^{3+} complex as a sensor for F^{-}, *Talanta*, 2019, **203**, 178–185, DOI: 10.1016/j.talanta.2019.05.051, https://www.ncbi.nlm.nih.gov/pubmed/31202324.

8 Y. Cheng, A. E. Clark, J. Zhou, T. He, Y. Li, R. M. Borum, M. N. Creyer, M. Xu, Z. Jin, J. Zhou, W. Yim, Z. Wu, P. Fajtova, A. J. O'Donoghue, A. F. Carlin and J. V. Jokerst, Protease-Responsive Peptide-Conjugated Mitochondrial-Targeting AIEgens for Selective Imaging and Inhibition of SARS-CoV-2-Infected Cells, *ACS Nano*, 2022, **16**, 12305–12317, DOI: 10.1021/acsnano.2c03219, https://www.ncbi.nlm.nih.gov/pubmed/35878004.

9 J. Luo, Z. Xie, J. W. Lam, L. Cheng, H. Chen, C. Qiu, H. S. Kwok, X. Zhan, Y. Liu, D. Zhu and B. Z. Tang, Aggregation-induced emission of 1-methyl-1,2,3,4,5-pentaphenylsilole, *Chem. Commun.*, 2001, 1740–1741, DOI: 10.1039/b105159h, https://www.ncbi.nlm.nih.gov/pubmed/12240292.

10 R. Hu, Z. Zhao, Z. Liu and B. Z. Tang, AIE biomaterials open up a promising arena for biomedical applications, *Biomaterials*, 2023, **297**, 122119–122120, DOI: 10.1016/j.biomaterials.2023.122119.

11 P. Alam, N. L. C. Leung, H. Su, Z. Qiu, R. T. K. Kwok, J. W. Y. Lam and B. Z. Tang, A Highly Sensitive Bimodal Detection of Amine Vapours Based on Aggregation Induced Emission of 1,2-Dihydroquinoxaline Derivatives, *Chemistry*, 2017, **23**, 14911–14917, DOI: 10.1002/chem.201703253. https://www.ncbi.nlm.nih.gov/pubmed/28796370.

12 K.-R. Zhang, M. Hu, J. Luo, F. Ye, T.-T. Zhou, Y.-X. Yuan, M.-L. Gao and Y.-S. Zheng, Pseudo-crown ether having AIE and PET effects from a TPE-CD conjugate for highly selective detection of mercury ions, *Chin. Chem. Lett.*, 2022, **33**, 1505–1510.

13 F.-Y. Ye, M. Hu, W. Yu and Y.-S. Zheng, Highly selective detection of palladium ions by sulfur-containing tetraphenylethylene tetracycle helicate, *Dyes Pigm.*, 2023, **208**, 110857, DOI: 10.1016/j.dyepig.2022.110857.

14 T. Harada, K. Sano, K. Sato, R. Watanabe, Z. Yu, H. Hanaoka, T. Nakajima, P. L. Choyke, M. Ptaszek and H. Kobayashi, Activatable organic near-infrared fluorescent probes based on a bacteriochlorin platform: synthesis and multicolor in vivo imaging with a single excitation, *Bioconjugate Chem.*, 2014, **25**, 362–369, DOI: 10.1021/bc4005238. https://www.ncbi.nlm.nih.gov/pubmed/24450401.

15 L. He, B. Dong, Y. Liu and W. Lin, Fluorescent chemosensors manipulated by dual/triple interplaying sensing mechanisms, *Chem. Soc. Rev.*, 2016, **45**, 6449–6461, DOI: 10.1039/c6cs00413j. https://www.ncbi.nlm.nih.gov/pubmed/27711651.

16 L. Peng, L. Xiao, Y. Ding, Y. Xiang and A. Tong, A simple design of fluorescent probes for indirect detection of beta-lactamase based on AIE and ESIPT processes, *J. Mater. Chem. B*, 2018, **6**, 3922–3926, DOI: 10.1039/c8tb00414e. https://www.ncbi.nlm.nih.gov/pubmed/32254320.

17 S. Tian, H. Bai, S. Li, Y. Xiao, X. Cui, X. Li, J. Tan, Z. Huang, D. Shen, W. Liu, P. Wang, B. Z. Tang and C. S. Lee, Water-Soluble Organic Nanoparticles with Programable Intermolecular Charge Transfer for NIR-II Photothermal Anti-Bacterial Therapy, *Angew. Chem., Int. Ed.*, 2021, **60**, 11758–11762, DOI: 10.1002/anie.202101406. https://www.ncbi.nlm.nih.gov/pubmed/33724623.

18 Z. Zhao, W. He and B. Z. Tang, Aggregate Materials beyond AIEgens, *Acc. Mater. Res.*, 2021, **2**, 1251–1260, DOI: 10.1021/accountsmr.1c00202.

19 W. Cao, H. Chen, Y. Yu, N. Li and W. Chen, Changing profiles of cancer burden worldwide and in China: a secondary analysis of the global cancer statistics 2020, *Chin Med. J. (Engl.)*, 2021, **134**, 783–791, DOI: 10.1097/CM9.0000000000001474. https://www.ncbi.nlm.nih.gov/pubmed/33734139.

20 S. Zhang, K. Sun, R. Zheng, H. Zeng, S. Wang, R. Chen, W. Wei and J. He, Cancer incidence and mortality in China, 2015, *J. Natl. Cancer Cent.*, 2021, **1**, 2–11, DOI: 10.1016/j.jncc.2020.12.001.

21 R. Zheng, S. Zhang, H. Zeng, S. Wang, K. Sun, R. Chen, L. Li, W. Wei and J. He, Cancer incidence and mortality in China, 2016, *J. Natl. Cancer Cent.*, 2022, **2**, 1–9, DOI: 10.1016/j.jncc.2022.02.002.

22 WHO, *WHO Report on Cancer: Setting Priorities, Investing Wisely and Providing Care for All*, 2020.

23 F. Cui, J. Bao and L. Wang, Analysis on the Trends and Projections of Disease Burden of Breast Cancer and Cervical Cancer among Women in China, from 1990 to 2019, *Chin. J. Health Statistics*, 2022, **39**, 647–652.

24 K. Sun, R. S. Zheng, S. W. Zhang, H. M. Zeng, X. N. Zou, R. Chen, X. Y. Gu, W. Wen Qiang and J. He, Report of Cancer Incidence and Mortality in Different Areas of China, *China Cancer*, 2019, **28**, 1–11, DOI: 10.11735/j.issn.1004-0242.2019.01.A001.

25 Y. Z. Jiang, D. Ma, C. Suo, J. Shi, M. Xue, X. Hu, Y. Xiao, K. D. Yu, Y. R. Liu, Y. Yu, Y. Zheng, X. Li, C. Zhang, P. Hu, J. Zhang, Q. Hua, J. Zhang, W. Hou, L. Ren, D. Bao, B. Li, J. Yang, L. Yao, W. J. Zuo, S. Zhao, Y. Gong, Y. X. Ren, Y. X. Zhao, Y. S. Yang, Z. Niu, Z. G. Cao, D. G. Stover, C. Verschraegen, V. Kaklamani, A. Daemen, J. R. Benson, K. Takabe, F. Bai, D. Q. Li, P. Wang, L. Shi, W. Huang and Z. M. Shao, Genomic and Transcriptomic Landscape of Triple-Negative Breast Cancers: Subtypes and Treatment Strategies, *Cancer Cell*, 2019, **35**, 428–440, DOI: 10.1016/j.ccell.2019.02.001. https://www.ncbi.nlm.nih.gov/pubmed/30853353.

26 W. He, Z. Zhang, Y. Luo, R. T. K. Kwok, Z. Zhao and B. Z. Tang, Recent advances of aggregation-induced emission materials for fluorescence image-guided surgery, *Biomaterials*, 2022, **288**, 121709, DOI: 10.1016/j.biomaterials.2022.121709, https://www.ncbi.nlm.nih.gov/pubmed/35995625.

27 E. Laurent, H. Begueret, B. Bonhomme, R. Veillon, M. Thumerel, V. Velasco, V. Brouste, S. Hoppe, M. Fournier, T. Grellety and G. MacGrogan, SOX10, GATA3, GCDFP15, Androgen Receptor, and Mammaglobin for the Differential Diagnosis Between Triple-negative Breast Cancer and TTF1-negative Lung Adenocarcinoma, *Am. J. Surg. Pathol.*, 2019, **43**, 293–302.

28 K. Karamanou, M. Franchi, D. Vynios and S. Brézillon, Epithelial-to-mesenchymal transition and invadopodia markers in breast cancer: Lumican a key regulator, *Semin. Cancer Biol.*, 2020, **62**, 125–133.

29 L. S. Ma, C. Y. Jiang, M. Cui, R. Lu, S. S. Liu, B. B. Zheng, L. Li and X. Li, Fluopsin C induces oncosis of human breast adenocarcinoma cells, *Acta Pharmacol. Sin.*, 2013, **34**, 1093–1100, DOI: 10.1038/aps.2013.44. https://www.ncbi.nlm.nih.gov/pubmed/23708552.

30 S. Pan, X. Zhao, C. Shao, B. Fu, Y. Huang, N. Zhang, X. Dou, Z. Zhang, Y. Qiu, R. Wang, M. Jin and D. Kong, STIM1 promotes angiogenesis by reducing exosomal miR-145 in breast cancer MDA-MB-231 cells, *Cell Death Dis.*, 2021, **12**, 38, DOI: 10.1038/s41419-020-03304-0. https://www.ncbi.nlm.nih.gov/pubmed/33414420.

31 N. A. Razak, N. Abu, W. Y. Ho, N. R. Zamberi, S. W. Tan, N. B. Alitheen, K. Long and S. K. Yeap, Cytotoxicity of eupatorin in MCF-7 and MDA-MB-231 human breast cancer cells via cell cycle arrest, anti-angiogenesis and induction of apoptosis, *Sci. Rep.*, 2019, **9**, 1514, DOI: 10.1038/s41598-018-37796-w. https://www.ncbi.nlm.nih.gov/pubmed/30728391.

32 P. Alam, W. He, N. L. C. Leung, C. Ma, R. T. K. Kwok, J. W. Y. Lam, H. Herman, Y. Sung, I. D. Williams, K. S. Wong and B. Z. Tang, Red AIE-Active Fluorescent Probes with Tunable Organelle-Specific Targeting, *Adv. Funct. Mater.*, 2020, **30**, 19092268, DOI: 10.1002/adfm.201909268.

33 G. M. Cragg and D. J. Newman, Natural products: a continuing source of novel drug leads, *Biochim. Biophys. Acta*, 2013, **1830**, 3670–3695, DOI: 10.1016/j.bbagen.2013.02.008. https://www.ncbi.nlm.nih.gov/pubmed/23428572.

34 C. Xia, X. Dong, H. Li, M. Cao, D. Sun, S. He, F. Yang, X. Yan, S. Zhang, N. Li and W. Chen, Cancer statistics in China and United States, 2022: profiles, trends, and determinants, *Chin. Med. J. (Engl.)*, 2022, **135**, 584–590, DOI: 10.1097/CM9.0000000000002108. https://www.ncbi.nlm.nih.gov/pubmed/35143424.

35 T. Khan and P. Gurav, PhytoNanotechnology: Enhancing Delivery of Plant Based Anti-cancer Drugs, *Front. Pharmacol*, 2017, **8**, 1–14, DOI: 10.3389/fphar.2017.01002. https://www.ncbi.nlm.nih.gov/pubmed/29479316.

36 Y. Liu, Z. Song, Y. Liu, X. Ma, W. Wang, Y. Ke, Y. Xu, D. Yu and H. Liu, Identification of ferroptosis as a novel mechanism for antitumor activity of natural product derivative a2 in gastric cancer, *Acta Pharm. Sin. B*, 2021, **11**, 1513–1525, DOI: 10.1016/j.apsb.2021.05.006. https://www.ncbi.nlm.nih.gov/pubmed/34221865.

37 W. Zhang, C. Liu, J. Li, Y. Lu, H. Li, J. Zhuang, X. Ren, M. Wang and C. Sun, Tanshinone IIA: New Perspective on the Anti-Tumor Mechanism of A Traditional Natural Medicine, *Am. J. Chin. Med.*, 2022, **50**, 209–239, DOI:

10.1142/S0192415X22500070. https://www.ncbi.nlm.nih.gov/pubmed/34983327.

38 J. Mei, Y. Hong, J. W. Lam, A. Qin, Y. Tang and B. Z. Tang, Aggregation-induced emission: the whole is more brilliant than the parts, *Adv. Mater.*, 2014, **26**, 5429–5479, DOI: 10.1002/adma.201401356. https://www.ncbi.nlm.nih.gov/pubmed/24975272.

39 Z. Wang, X. Zeng, G. Yang, X. Cao, S. Luo, C. Qi and S. Chen, Progress in Design, Synthesis and Application of Triphenylamine-Based Fluorescent Probes, *Chin. J. Org. Chem.*, 2021, **41**(3), 919–933, DOI: 10.6023/cjoc202009012.

40 P. Gayathri, M. Pannipara, A. G. Al-Sehemi and S. P. Anthony, Triphenylamine-based stimuli-responsive solid state fluorescent materials, *New J. Chem.*, 2020, **44**, 8680–8696, DOI: 10.1039/d0nj00588f.

41 Y. Li, S. Liu, H. Ni, H. Zhang, H. Zhang, C. Chuah, C. Ma, K. S. Wong, J. W. Y. Lam, R. T. K. Kwok, J. Qian, X. Lu and B. Z. Tang, ACQ-to-AIE Transformation: Tuning Molecular Packing by Regioisomerization for Two-Photon NIR Bioimaging, *Angew Chem., Int. Ed.*, 2020, **59**, 12822–12826, DOI: 10.1002/anie.202005785. https://www.ncbi.nlm.nih.gov/pubmed/32385974.

42 F. Meng, C. Zheng, Y. Li, L. Sun, X. Liu, T. Zhang and H. Piao, Synthesis and Anti-bacterial Activity of Novel Chalcone Derivatives Containing 2,4-Thiazolidinedione-3-acetic Acid Moiety, *Chin. J. Org. Chem.*, 2012, **32**, 183–187, DOI: 10.6023/cjoc1107182.

43 L. BeiBei, G. Y. He, Z. G. Hu and F. J. Zeng, Research progress of thiazolidinediones and lung cancer, *BACHU Med Journal*, 2019, **2**, 115–118.

44 Z. Yu and J. B. Liu, Synthesis and Tyrosinase-inhibitory Activities of Novel Thiazolidinedione Derivatives, *Chin. J. Synth. Chem.*, 2021, **29**, 650–655.

45 Y. Ma, H. A. Aisha, L. Liao, S. Aibai, T. Zhang and Y. Ito, Preparative isolation and purification of rupestonic acid from the Chinese medicinal plant *Artemisia rupestris* L. by high-speed counter-current chromatography, *J. Chromatogr. A*, 2005, **1076**, 198–201, DOI: 10.1016/j.chroma.2005.04.040. https://www.ncbi.nlm.nih.gov/pubmed/15974089.

46 E. Ferrero, I. Dunham and P. Sanseau, In silico prediction of novel therapeutic targets using gene-disease association data, *J. Transl. Med.*, 2017, **15**, 182, DOI: 10.1186/s12967-017-1285-6. https://www.ncbi.nlm.nih.gov/pubmed/28851378.

47 A. Abu Bakar, M. Akhtar, N. Mohd Ali, S. Yeap, C. Quah, W.-S. Loh, N. Alitheen, S. Zareen, Z. Ul-Haq and S. Shah, Design, Synthesis and Docking Studies of Flavokawain B Type Chalcones and Their Cytotoxic Effects on MCF-7 and MDA-MB-231 Cell Lines, *Molecules*, 2018, **23**, 616, DOI: 10.3390/molecules23030616.

48 E. Aydin, A. M. Senturk, H. B. Kucuk and M. Guzel, Cytotoxic Activity and Docking Studies of 2-arenoxybenzaldehyde N-acyl Hydrazone and 1,3,4-Oxadiazole Derivatives against Various Cancer Cell Lines, *Molecules*, 2022, **27**, DOI: 10.3390/molecules27217309. https://www.ncbi.nlm.nih.gov/pubmed/36364134.

49 X. Liu, J. Liang, Y. Yu, X. Han, L. Yu, F. Chen, Z. Xu, C. Qi, M. Jin, C. Dong, H.-B. Zhou, K. Lan and S. Wu, Discovery of Aryl Benzoyl Hydrazide Derivatives as Novel Potent Broad-Spectrum Inhibitors of Influenza A Virus RNA-Dependent RNA Polymerase (RdRp), *J. Med. Chem.*, 2022, **65**, 3814–3832, DOI: 10.1021/acs.jmedchem.1c01257. https://doi.org/10.1021/acs.jmedchem.1c01257.

50 A. E. Mohammed, F. Ameen, K. Aabed, R. S. Suliman, S. S. Alghamdi, F. A. Safhi, D. S. Alshaya, H. Ali Alafari, A. S. Jalal, A. A. Alosaimi, S. M. Alshamrani and I. Rahman, In-silico predicting as a tool to develop plant-based biomedicines and nanoparticles: Lycium shawii metabolites, *Biomed. Pharmacother.*, 2022, **150**, 113008, DOI: 10.1016/j.biopha.2022.113008.